Advanced Spatial Modulation Systems for Future MIMO Systems

by

Mehmet Akif Kurt

A Dissertation Submitted to the
Graduate School of Sciences and Engineering
in Partial Fulfillment of the Requirements for
the Degree of

Master of Science

in

Electrical and Electronics Engineering

KOÇ ÜNİVERSİTESİ

July 27 , 2022

Advanced Spatial Modulation Systems for Future MIMO Systems

Koç University

Graduate School of Sciences and Engineering

This is to certify that I have examined this copy of a master's thesis by

Mehmet Akif Kurt

and have found that it is complete and satisfactory in all respects,
and that any and all revisions required by the final
examining committee have been made.

Committee Members:

Assoc. Prof. Ertugrul Basar (Advisor)

Prof. Alper Erdogan

Assoc. Prof. Erdogan Aydın

Date:

Dedicated to my dear family

ABSTRACT

Advanced Spatial Modulation Systems for Future MIMO Systems
Mehmet Akif Kurt
Master of Science in Electrical and Electronics Engineering
July 27 , 2022

Spatial modulation (SM) seems like a promising transmission technique for multiple-input multiple-output (MIMO) systems to meet the requirements of future wireless communication technologies. SM activates only one transmit antenna in each time slot and conveys additional information bits through the indices of active transmit antennas. Thus, the spectral efficiency increases without increasing the modulation order. Besides, SM requires only one radio frequency (RF) chain, which means low-level hardware complexity and inter-channel interference (ICI) cancellation due to the activation of only one transmit antenna. In recent years, the design of SM-based transmission techniques has become a general research topic because of the advantages of SM, and it is seen that clever SM-based designs can increase the spectral efficiency and bit error rate (BER) performance concerning SM. In this thesis, three novel SM-based transmission schemes are proposed for next-generation MIMO systems.

Firstly, a novel transmission scheme named transmit antenna grouping quadrature SM (TAG-QSM) is proposed. The motivation of TAG-QSM is to increase the number of information bits in the spatial domain to achieve lower modulation order than the existing schemes in the literature. In TAG-QSM, transmit antenna groups with an equal number of transmit antennas are created. After that, first, the incoming bit group determines the indices of transmit antenna groups separately for the transmission of the real and imaginary parts of data symbol. The second incoming bit group chooses one transmit antenna from each of the determined transmit antenna groups. Data symbol is determined using the last bit group. To conclude, the increase in the number of additional information bits in the spatial domain results in lower modulation order and improved BER performance concerning the benchmark schemes. In this study, the theoretical upper bound is derived for BER, and Monte Carlo simulations are demonstrated for comparing the BER performance of TAG-

QSM with the benchmark schemes and showing the consistency of the theoretical upper bound of BER derivation.

Secondly, flexible spatial modulation with transmit antenna selection (FSM-TAS) is introduced for future multiple-input multiple-output (MIMO) systems. In this scheme, the number of active antennas varies in each time slot depending on the incoming bits. After determining the number of active antennas, channel coefficients corresponding to each possible active antenna combination are added up. Then, a certain number of antenna combinations with largest gains is selected to apply spatial modulation (SM). For the proposed system, complexity and outage probability analyses are performed. In addition, it has been shown by Monte Carlo simulations that FSM-TAS provides better bit error rate (BER) performance than the benchmark scheme, named enhanced spatial modulation with generalized antenna selection (ESM-GAS) [Qing et al., 2021], under the same spectral efficiency, the same number of transmitter and receiver antennas.

Thirdly, spatial modulation (SM) using signal space diversity (SM-SSD) is proposed for multiple-input multiple-output (MIMO) systems. In this scheme, consecutive time slots are processed jointly and signal and space diversity (SSD) technique is applied for the transmission of data symbols to obtain transmit diversity. In addition, a clever active antenna activation algorithm is introduced to prevent transmit diversity degradation. An upper bound BER derivation is performed and compared with Monte Carlo simulations. Besides, BER performance comparison is demonstrated with the reference schemes in the literature. Lastly, the suboptimal solution for the rotation angles is expressed to maximize minimum coding gain distance (MCGD).

ÖZETÇE

Yüksek Lisans Tez Başlığı
Mehmet Akif Kurt
Elektrik ve Elektronik Mühendisliği, Yüksek Lisans
27 Temmuz 2022

Uzaysal modülasyon (SM) tekniği, geleceğin kablosuz iletişim teknolojilerinin gereksinimlerini karşılamak adına çok girişli çok çıkışlı (MIMO) sistemler için umut verici bir iletim tekniği olarak gözükmektedir. SM, her zaman diliminde yalnızca bir verici anteni etkinleştirir ve aktif verici antenin indissleri aracılığıyla ek bilgi bitlerini iletmektedir. Böylece, M olan bir modülasyon seviyesi artırılmadan spektral verimlilik artırılmaktadır. Ayrıca, SM yalnızca bir radyo frekansı (RF) zinciri gerektirmektedir; bu, yalnızca bir verici antenin etkinleştirilmesi nedeniyle düşük seviyeli donanım karmaşıklığı ve kanallar arası parazit (ICI) iptali anlamına gelmektedir. Son yıllarda, SM'nin avantajları nedeniyle SM tabanlı iletim tekniklerinin tasarımı genel bir araştırma konusu haline gelmiştir ve akıllı SM tabanlı tasarımların, ilgili spektral verimliliği ve bit hata oranı (BER) performansını artırabileceği görülmektedir. SM. Bu tezde, yeni nesil MIMO sistemleri için üç özgün SM tabanlı iletim şeması önerilmektedir.

İlk olarak, yeni bir iletim şeması olan verici anten gruplamalı dik SM (TAG-QSM) önerilmektedir. TAG-QSM'nin motivasyonu, uzaysal alandaki bilgi bitlerinin sayısını arttırarak literatürdeki mevcut şemalardan daha düşük modülasyon seviyesi elde etmektir. TAG-QSM'de eşit sayıda verici antene sahip verici anten grupları oluşturulmaktadır. Daha sonra, ilk bit grubu, simgenin gerçek ve sanal kısımlarının iletimi için ayrı ayrı verici anten gruplarının indislerini belirlemektedir. Gelen ikinci bit grubu, belirlenen verici anten gruplarının her birinden bir verici anten seçmektedir. İletilen simge, son bit grubu kullanılarak belirlenmektedir. Sonuç olarak, uzaysal alanda iletilen bilgi bitlerinin sayısındaki artış, referans şemalara göre daha düşük modülasyon seviyesi ve iyileştirilmiş BER performansı olarak sonuçlanmaktadır. Bu çalışmada, BER için teorik üst sınır elde edilmiştir ve TAG-QSM'nin BER performansını referans şemalar ile karşılaştırmak ve teorik BER üst sınırının tutarlılığını göstermek için Monte Carlo simülasyonları yapılmıştır.

İkinci olarak, gelecek nesil çok girişli çok çıkışlı (MIMO) sistemleri için verici anten seçimli esnek uzaysal modülasyon (FSM-TAS) tanıtılmaktadır. Bu şemada, aktif antenlerin sayısı, gelen bitlere bağlı olarak her zaman aralığında değişir. Aktif anten sayısı belirlendikten sonra, olası her aktif anten kombinasyonuna karşılık gelen kanal katsayıları toplanır. Daha sonra, en büyük kazançlara sahip belirli sayıda anten kombinasyonu SM uygulamak için seçilmektedir. Önerilen sistem için karmaşıklık ve kesinti olasılığı analizleri yapılmıştır. Ayrıca, FSM-TAS'ın aynı spektral verimlilik, aynı sayıda verici altında genelleştirilmiş anten seçimli iyileştirilmiş uzamsal modülasyondan (ESM-GAS) daha iyi bit hata oranı (BER) performansı sağladığı Monte Carlo simülasyonları ile gösterilmiştir.

Üçüncü olarak, çok girişli çok çıkışlı (MIMO) sistemler için sinyal alanı çeşitliliğini kullanan sinyal ve uzay çeşitlemeli uzaysal modülasyon (SM-SSD) önerilmektedir. Bu şemada ardışık zaman dilimleri birlikte işlenmekte ve iletim çeşitliliği amacıyla veri sembollerinin iletiminde sinyal ve uzay çeşitleme (SSD) tekniği uygulanmaktadır. Ek olarak, çoğullama çeşitliliği bozulmasını önlemek için akıllı bir aktif anten aktivasyon algoritması tanıtılmaktadır. Üst sınır türetme yapılır ve Monte Carlo simülasyonları ile karşılaştırılmaktadır. Ayrıca BER performans karşılaştırması literatürdeki referans şemalar ile gösterilmiştir. Son olarak, minimum kodlama kazanç mesafesi (MCGD) kriterlerini maksimize etmek için döndürme açıları için alt optimal çözüm ifade edilmiştir.

ACKNOWLEDGMENTS

I would like to thank my dear advisor Dr. Ertuğrul Başar for his support, trust and patience. He does not only push me for better academic results but also always treats me kindly and this makes me feel valued. I feel very lucky to be student of him.

I would also like to thank to my dear father Orhan, my lovely mother Sebahat, my sister Eda and my brother Oğuzhan for their continuous support and love. They always motivate me to do my best.

I would like to thank to my friend group, named "boş", for their sincere friendship. They always show their support and make my life enjoyable .

I would like to thank my friends in CoreLab. We had a great year after pandemic. I wish there were no pandemic and we met earlier.

Lastly, I also want to thank The Scientific and Technological Research Council of Turkey (TUBITAK) for supporting me during my MSc study through 2210-A National Scholarship Programme.

TABLE OF CONTENTS

LIST OF TABLES

LIST OF FIGURES

ABBREVIATIONS

AAP	Antenna Activation Pattern
ABEP	Average Bit Error Probability
BER	Bit Error Rate
CA	Complex Addition
CDF	Cumulative Distribution Function
CM	Complex Multiplication
COAS	Capacity Optimized Antenna Selection
CPEP	Conditional Pairwise Error Probability
CSI	Channel State Information
EDAS	Euclidian Distance Antenna Selection
GSM	Generalized Spatial Modulation
ICI	Inter-Channel Interference
IEEE	The Institute of Electrical and Electronics Engineers
IM	Index Modulation
MCGD	Minimum Coding Gain Distance
MGF	Moment Generating Function
MIMO	Multiple-Input Multiple-Output
ML	Maximum Likelihood
QAM	Quadrature Amplitude Modulation
QSM	Quadrature Spatial Modulation
PCSI	Perfect Channel State Information
PDF	Probability Density Function
PEP	Pairwise Error Probability
PSK	Phase Shift Keying
RF	Radio Frequency
SISO	Single-Input Single-Output
SM	Signal-to-Noise Ratio
SMX	Spatial Multiplexing
SSD	Signal Space Diversity
STBC	Space Time Block Coding

Chapter 1

INTRODUCTION

Achieving higher data rates and enhancing the capacity of the communication systems are the requirements of next-generation communication networks. Multiple-input multiple-output (MIMO) systems are promising to achieve the requirements of the next-generation communication networks since MIMO systems are more capable than single-input single-output (SISO) systems to meet the requirements of the next-generation communication networks. The effective design of MIMO systems is one of the active research topics in the past two decades. Space-time block coding (STBC) and spatial multiplexing (SMX) transmission techniques are proposed to provide diversity and multiplexing gains. The information is transmitted over different antennas in different time slots with STBC, and a transmit diversity is obtained. SMX transmission techniques aim to transmit more than one data symbol over the transmitter antennas. Vertical Bell Labs layered space-time (V-BLAST) [Foschini, 1996] which is one of the most popular SMX techniques, activates all transmit antennas, and each antenna transmits a different data symbol. In this way, the spectral efficiency increases proportionally with the number of transmit antennas, and the transmit diversity is obtained. However, the number of required radio frequency (RF) chains increases with the number of transmit antennas, and inter-channel interference (ICI) and the receiver complexity have occurred.

Index modulation (IM) has been regarded as a novel approach for MIMO systems since a significant increase in spectral efficiency, and energy efficiency can be achieved without high-level receiver complexity [Basar et al., 2017] -[Basar, 2016]. In recent years, for the IM concept, spatial modulation (SM) [Mesleh et al., 2006] has become popular. SM carries information bits to activate one transmit antenna at each time slot in addition to the M-QAM/PSK constellation symbols. In this way, inter-channel interference (ICI) is avoided with a low-level receiver complexity.

In this thesis, three novel SM-based transmission schemes are proposed for the next generation MIMO systems.

1.1 Contributions of the Thesis

In this thesis, firstly, a novel SM-based transmission scheme named transmit antenna grouping QSM, which aims to increase the number of information bits with the indices of the active transmit antennas, is proposed. In TAG-QSM [Kurt and Basar, 2021], the transmit antennas are divided into groups equally. The transmit antenna groups are determined separately by considering incoming bits for the real and imaginary parts. Then, the transmit antennas are activated from the determined transmit antenna groups concerning incoming bits. The variation in the number of active antennas for the transmission of data symbol enables higher data rates in the spatial domain possible concerning the benchmark schemes in the literature. As a result, TAG-QSM can achieve the same data rates with a lower modulation order, which enhances the error performance.

Secondly, flexible SM with transmit antenna selection for MIMO systems (FSM-TAS) is proposed. In FSM-TAS [Kurt and Basar, 2022], the number of active transmit antennas is determined concerning the incoming bits first. In the next step, the combinations of the channel coefficients with the determined number of active antennas are sorted by considering the squared norms. Then, a number of channel coefficient combinations with higher gains are selected to apply SM. Lastly, SM is applied, and one channel coefficient combination is determined for the transmission of data symbol. By determining the number of the active antennas depending on the incoming bits and making squared norm-based transmit antenna selection, FSM-TAS conveys more data bits with IM and provides better error performance than the benchmark schemes.

Lastly, SM using signal space diversity (SM-SSD) is introduced. SM-SSD modulates consecutive time slots jointly and applies SSD technique to transmit data symbols, which are determined from the rotated M-QAM/PSK constellations. SSD is applied by shifting the imaginary parts of data symbol with respect to the incoming bits. Besides, the antenna activation patterns (AAPs) are created cleverly to enhance the transmit diversity concerning the benchmark schemes. The enhancement in the transmitter diversity results in error performance improvement.

The contributions of this thesis are submitted as three short papers. TAG-QSM has been presented in Institute of Electrical and Electronics Engineers (IEEE) 29. Signal Processing and Communications Applications Conference (SIU 2021). FSM-TAS has been accepted for publication in IEEE Systems Journal. Finally, the work involving SM-SSD has been submitted to IEEE Communications Letters.

Notation: Bold, lowercase and capital letters describe column vectors and matrices, respectively. $\text{rank}(\mathbf{X})$ denote the rank of $\mathbf{X}$. $[.]^H$,$[.]^T$,$||.||$, $\binom{:}{:}$ represent Hermitian, transpose, Euclidian norm, and the binomial coefficient respectively. $\mathcal{CN}(m_x, \sigma_x^2)$ is Gaussian distribution with mean m_x and variance σ_x^2.

Chapter 2

SPATIAL MODULATION

In this chapter, a novel transmission scheme, called SM [Mesleh et al., 2006], is proposed for MIMO systems. In SM, only one transmit antenna is activated for data transmission; thus, only one RF chain would be enough, and ICI is canceled. Besides, the information bits are not only conveyed through M-QAM/PSK symbols but also over active transmit antenna indices. In this way, SM increases the spectral efficiency without increasing the receiver complexity. Using only one RF chain, an increase in spectral efficiency and lower receiver complexity are the main advantages of SM, and SM is promising for the MIMO systems.

2.1 Working Principle of SM

SM considers $N_r \times N_t$ MIMO systems and M-QAM/PSK constellation where M is a modulation order, N_r and N_t are the number of receiver antennas and the number of transmit antennas, respectively. The spectral efficiency of the SM can be expressed as follows

$$\eta_{SM} = \log_2(M) + \log_2(N_t) \tag{2.1}$$

The incoming bit group with the length of $\log_2(N_t)$ determines the indice of the active antenna, a, and the incoming bit group with the length of $\log_2(M)$ determines data symbol, s. After data symbol and the indice of the active antenna are determined, the transmission vector, $\mathbf{x}$, is created. $\mathbf{x}$ is $N_t \times 1$ vector and has only one nonzero element. x can be shown as

$$\mathbf{x} = [0, 0, ..., 0, \underbrace{s}_{a}, 0, 0, ..., 0] \tag{2.2}$$

The received signal $\mathbf{y} \in \mathbb{C}^{N_r \text{x} 1}$ can be expressed as

$$\mathbf{y} = \sqrt{\rho}\mathbf{H}\mathbf{x} + \mathbf{n}, \tag{2.3}$$

where $\mathbf{H} \in \mathbb{C}^{N_r \text{x} N_t}$ is Rayleigh fading channel matrix, $\mathbf{n} \in \mathbb{C}^{N_R \text{x} 1}$ is additive white Gaussian noise vector with $\mathcal{CN}(0, 1)$, and ρ is average signal-to-noise ratio at each receiver antenna. SM estimates the active antenna indice and data symbol using maximum likelihood (ML) detector. The detector works as follows

$$[\hat{a}, \hat{s}] = \arg\min_{a,s} ||\mathbf{y} - \sqrt{\rho}\mathbf{H}\mathbf{x}||^2 \tag{2.4}$$

where $\hat{a}$, $\hat{s}$ are the estimated active antenna indice and data symbol, respectively.

2.2 A Literature Review on SM

Using only one transmit antenna at each time slot in SM decreases the efficiency of the use of multiple transmit antennas. To overcome this issue, generalized SM (GSM) is proposed [Wang et al., 2012], [Younis et al., 2010] and [Datta et al., 2015]. GSM transmits an M-ary symbol with more than one active transmit antenna in each time slot. Thus, the transmit antennas are used in a more effective way without ICI since the same symbol is transmitted over all active antennas. In [Mesleh et al., 2006], low complex, but not optimum detector is proposed. On the other hand, maximum likelihood (ML) detector, which is optimum for SM, is proposed in [Jeganathan et al., 2008]. Quadrature spatial modulation (QSM) [Mesleh et al., 2014] also aims to increase the spectral efficiency by keeping the advantages of the SM, such as low-level receiver complexity and ICI cancellation. In QSM, data symbol is divided into real and imaginary parts. The incoming bits activate one transmit antenna for the real and imaginary parts separately; thus, the number of bits conveyed in the spatial domain increases concerning the SM. In [Yigit and Basar, 2016], double SM (DSM) is proposed to have diversity gain, and to increase spctral efficiency by activating more transmit antenna than SM. Parallel QSM (PQSM) [Huang et al., 2019] uses the QSM principlee and sends the real and imaginary parts of data symbol over the different transmit antennas. Different from QSM, the transmit antennas are divided into groups equally, and one antenna is activated from each transmit group for the real and imaginary parts separately. In this way, PQSM has a more flexible structure than QSM in terms of the use of the transmit antennas and is more spectrally efficient than QSM. The principle of SM [Mesleh et al., 2006] is also applied to optical wireless communication in [Mesleh et al., 2011],[Popoola et al., 2013] and [Vlădeanu et al., 2012].

Enhanced approaches, which are capacity-optimized antenna selection (COAS) and Euclidian distance antenna selection (EDAS), are introduced in [Rajashekar et al., 2013] -[Pillay and Xu, 2013] for SM-based MIMO systems. Both COAS and EDAS schemes require channel state information (CSI) at both transmitter and receiver. COAS selects a subgroup of transmit antennas with higher channel gains to apply the SM. On the other hand, EDAS aims to maximize Euclidian distance and selects a subgroup of the transmit antennas by considering this criterion. Despite their higher modulation order of COAS and EDAS, both of them outperform the SM in error performance.nIn [Yang et al., 2016], the advantages of transmit antenna selection (TAS) algorithms on SM are discussed. Then, QR decomposition (QRD)-based TAS (QRD-TAS) and the error-vector magnitude-based TAS (EVM-TAS), which provide better BER performances with lower complexity, are proposed. An outage probability analysis for SM with TAS, which aims to maximize the power of the received signal over Rayleigh fading channel, is performed in [Kumbhani and Kshetrimayum, 2014], and a closed-form expression is shown. In [Qing et al., 2021], enhanced SM with generalized antenna selection (ESM-GAS) is introduced. ESM-GAS scheme sorts squared-norm values of all possible combinations of channel coefficients at each time slot and selects a subgroup of these combinations with higher norm to apply SM. In this way, ESM-GAS uses transmit antennas more efficiently to maximize the received signal power. However, sorting all possible combinations significantly increases the transmitter and receiver complexities. Space-time coding (STC) schemes activate multiple transmit antennas and modulate data symbols. In this way, STC schemes provide transmit diversity and improve the BER performance [Alamouti, 1998, Li and Wang, 2014, Jeon and Lee, 2015]. However, modulating more than one data symbol increases the required number of radio frequency (RF) chains. Thus, these schemes have higher hardware complexity at the transmitter side than SM schemes. Signal space diversity (SSD) is a new diversity technique that interleaves the real and imaginary parts of data symbols for Rayleigh fading channels [Boutros and Viterbo, 1998]. SSD is applied for SM-based transmission schemes to improve the BER performance through the transmit diversity enhancement and to decrease hardware complexity by using only one RF chain [Althunibat and Mesleh, 2018, Yang et al., 2019]. In these schemes, data symbols are selected from rotated constellations. After that, the real and imaginary parts are transmitted over consecutive time slots. With this methodology, higher diversity orders are obtained with a single RF chain, which is one of the main properties of SM..

Chapter 3

TRANSMIT ANTENNA GROUPING QUADRATURE SPATIAL MODULATION FOR MIMO SYSTEMS

It is clear that QSM conveys more information bits with IM than SM since QSM determines transmit antennas for real and imaginary parts of data symbol separately. In this way, QSM can achieved same spectral efficiency with lower modulation order. However, activating only one transmit antenna for real and imaginary parts also limits the spectral efficiency and it is not satisfactory. To overcome this issue, TAG-QSM is proposed in this chapter. TAG-QSM activates more than one than transmit antenna for the real and imaginary parts of data symbol separately. Transmit antennas are grouped and the activated antennas are determined from these transmit antenna groups depending on incoming bits. In this way, TAG-QSM aims to convey more information bits in the spatial domain and has lower modulation order.

In the rest of this chapter, system model of TAG-QSM is introduced, complexity and performance analyses are performed. Lastly, simulation results of BER performance of TAG-QSM are demonstrated.

3.1 System Model

In this section, a novel SM based transmission scheme TAG-QSM is proposed for a MIMO system with N_T transmit antennas, N_R receive antennas, M-ary constellation, and K transmit antenna groups where $N_T \geq K$ and N_T, K are power of two. The channel between transmitter and receiver follows Rayleigh fading and denoted as $\mathbf{H} \in \mathbb{C}^{N_R \times N_T}$, where $h_{i,j}$ with $i \in \{1, 2, ..., N_R\}$ and $j \in \{1, 2, ..., N_T\}$ represents channel gain between i-th receive and j-th transmit antennas, which is assumed to be an independent and identically distributed complex Gaussian random variable with $\mathcal{CN}(0,1)$ distribution. The system model of TAG-QSM can be seen in Fig. 3.1

3.1.1 Transmitter Side

At the transmitter, N_T transmit antennas are divided into K groups equally. Besides, S is the largest power of 2 which satisfies the condition that $S \leq \binom{K}{N_A}$. Incoming bits are divided into the 3 main groups as $\boldsymbol{b}_1$, $\boldsymbol{b}_2$, $\boldsymbol{b}_3$, and the lengths of the bit groups are $2\log_2 S$, $2N_A \log_2(\frac{N_T}{K})$, $\log_2 M$ respectively. The spectral efficiency in bits per channel use (bpcu) of the TAG-QSM can be expressed as

$$\eta = 2\log_2(S) + 2N_A \log_2(\frac{N_T}{K}) + \log_2(M). \tag{3.1}$$

The incoming bit group $\boldsymbol{b}_1$ is divided into two subgroups as $\boldsymbol{b}_{1r}$ and $\boldsymbol{b}_{1i}$. The

Table 3.1: Transmit antenna groups mapping for $K = 4$, $N_A = 2$, $S = 4$

$\boldsymbol{b}_{1r}$	$\boldsymbol{G}_r$
00	[1,2]
01	[1,3]
10	[1,4]
11	[2,3]

subgroups $\boldsymbol{b}_{1r}$ and $\boldsymbol{b}_{1i}$ determine N_A of K transmit antenna groups separately for the real and imaginary parts of data symbol, respectively. The indices of the determined transmit antenna groups for the transmission of the real part of data symbol can be given as

$$\mathbf{G}_r = [G_{r1}, G_{r2}, ..., G_{rN_A}]. \tag{3.2}$$

The indices of the determined transmit antenna groups for the transmission of the imaginary part of data symbol can be shown as

$$\mathbf{G}_i = [G_{i1}, G_{i2}, ..., G_{iN_A}]. \tag{3.3}$$

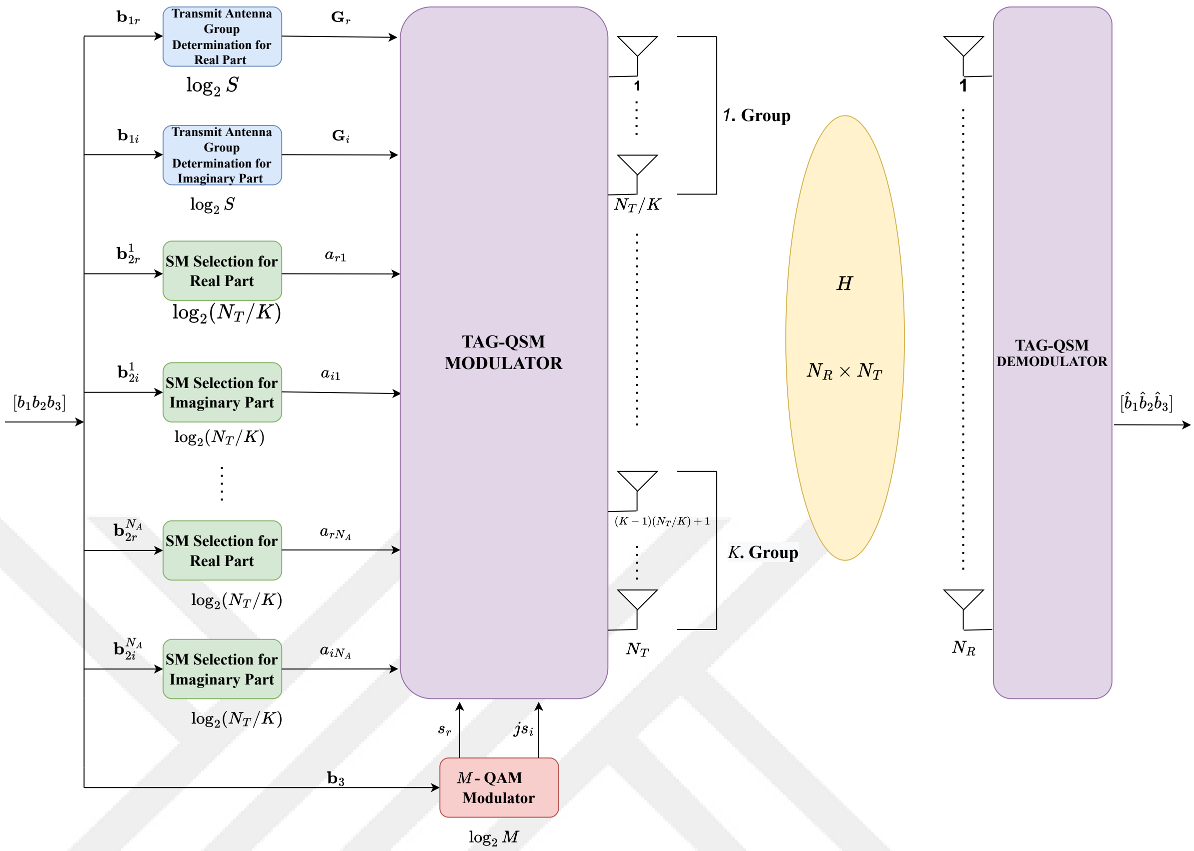

Figure 3.1: TAG-QSM System Model.

Table 3.1 is the look-up table for the determination of the $\mathbf{G}_r$ with respect to $\boldsymbol{b}_{1r}$ for $K = 4$ and $N_A = 2$. The table is also valid for the determination of the $\mathbf{G}_i$ with respect to $\boldsymbol{b}_{1i}$ bit group. The bit group $\boldsymbol{b}_2$ is divided into $2N_A$ subgroups as $\boldsymbol{b}_{2r}^t$, $t = \{1, 2, ..., N_A\}$ and $\boldsymbol{b}_{2i}^z$, $z = \{1, 2, ..., N_A\}$. $\boldsymbol{b}_{2r}^t$ activates one transmit antenna from the $\boldsymbol{G}_{rt}$-th transmit antenna group while $\boldsymbol{b}_{2r}^z$ activates one transmit antenna from $\boldsymbol{G}_{iz}$-th transmit antenna group. In this way, N_A transmit antennas are activated separately for the transmission of the real and imaginary parts of data symbol. The number of active transmit antennas varies between N_A and $2N_A$ in each time slot. The transmitted data symbol can be expressed as a sum of the real and imaginary parts as

$$s = s_r + js_i. \tag{3.4}$$

The indices of activated transmit antennas for transmission of the real and imaginary parts of data symbol can be seen in (3.5) and (3.6) respectively.

$$\mathbf{a}_r = [a_{r1}, a_{r2}, ..., a_{rN_A}]. \tag{3.5}$$

$$\mathbf{a}_i = [a_{i1}, a_{i2}, ..., a_{iN_A}]. \tag{3.6}$$

After determining $\mathbf{a}_r$, $\mathbf{a}_i$ and s, the transmission vector can be expressed as follows

$$\mathbf{x} = \frac{1}{\sqrt{N_A}}[0, 0, \underbrace{s_r}_{a_{r1}}, 0, ..., 0, \underbrace{js_i}_{a_{i1}}, 0, ..., \underbrace{s_r}_{a_{rN_A}}, 0, ..., 0, \underbrace{js_i}_{a_{iN_A}}, 0]^T \tag{3.7}$$

An example for transmission process of the TAG-QSM scheme with $N_T = 8$, $K = 4$ and $N_A = 2$ can be seen below.

Example: $N_T = 8$ transmit antennas are divided into $K = 4$ transmit antenna groups and $N_A = 2$ transmit antennas are activated for the transmission of the real and imaginary parts of data symbol separately. In case of 4-QAM, the spectral efficiency is 10 bpcu. Assume that the incoming bits are [0010001101]. Then, the incoming bits can be divided as $\boldsymbol{b}_1 = [0010]$, $\boldsymbol{b}_1 = [0011]$ and $\boldsymbol{b}_1 = [01]$. For $\boldsymbol{b}_1 = [0010]$, the subgroups can be shown as $\boldsymbol{b}_{1r} = [00]$ and $\boldsymbol{b}_{1i} = [10]$. By looking at Table 3.1, the indices of the transmit antenna groups for transmission of the real and imaginary parts can be found as $G_{r1} = 1$, $G_{r2} = 2$, $G_{i1} = 1$, $G_{i2} = 4$. $\boldsymbol{b}_2 = [0011]$ is divided into 4 subgroups as $\boldsymbol{b}_{2r}^1 = [0]$, $\boldsymbol{b}_{2i}^1 = [0]$, $\boldsymbol{b}_{2r}^2 = [1]$, $\boldsymbol{b}_{2i}^2 = [1]$. It means that the real part of data symbol is transmitted over the first antenna of the $G_{r1} = 1$ and the second antenna of the $G_{r2} = 2$ while the imaginary part is transmitted over the first antenna of the $G_{i1} = 1$ and the second antenna of the $G_{i2} = 4$. As a result, the active antenna indices are found as $a_{r1} = 1$, $a_{r2} = 4$, $a_{i1} = 1$, $a_{i2} = 8$. Lastly, $\boldsymbol{b}_3 = [01]$ determines data symbol as $s = -0.7 + j0.7$ and the real and imaginary parts can be shown as $s_r = -0.7$ and $s_i = 0.7$, respectively. After the active transmit antenna indices and data symbol are determined, the transmission vector can be obtained as

$$\mathbf{x} = \frac{1}{\sqrt{2}}[\underbrace{-0.7 + j0.7}_{a_{r1}=a_{i1}=1}, 0, 0, \underbrace{-0.7}_{a_{r2}=4}, 0, 0, 0, \underbrace{j0.7}_{a_{i2}=8}]^T \tag{3.8}$$

3.1.2 Receiver Side

The received signal $\mathbf{y} \in \mathbb{C}^{N_R \text{x} 1}$ at the receiver is given as follows

$$\mathbf{y} = \sqrt{\rho}\mathbf{H}\mathbf{x} + \mathbf{n}. \tag{3.9}$$

where $\mathbf{x} \in \mathbb{C}^{N_T \text{x} 1}$ is the transmission vector with $E[\mathbf{x}^H\mathbf{x}] = 1$, $\mathbf{n} \in \mathbb{C}^{N_R \text{x} 1}$ is additive white Gaussian noise vector with $\mathcal{CN}(0, 1)$, and ρ is average signal-to-noise ratio at each receiver antenna. It is assumed that the receiver has perfect channel state information (PCSI). $\boldsymbol{a}_r$, $\boldsymbol{a}_i$ and s are determined at the receiver using maximum likelihood (ML) detector. The detector works as below

$$[\hat{s}, \hat{\mathbf{a}}_r, \hat{\mathbf{a}}_i, \hat{\mathbf{G}}_r, \hat{\mathbf{G}}_i] = \underset{s, a_r, a_i, \mathbf{G}_r, \mathbf{G}_i}{\arg\min} ||\mathbf{y} - \sqrt{\rho}\mathbf{H}\mathbf{x}||^2. \tag{3.10}$$

where $\hat{\boldsymbol{a}}_r$, $\hat{\boldsymbol{a}}_i$, $\hat{\mathbf{G}}_i$, $\hat{\mathbf{G}}_i$ and $\hat{s}$ are the detected active antenna indices for the real part, the detected active antenna indices for the imaginary part, the detected transmit antenna groups for the real part, the detected transmit antenna groups for the imaginary part and the detected data symbol, respectively.

3.2 Performance Analysis

In this section, an upper bound of the BER of TAG-QSM system is obtained under the assumption of ML detection. As in [Simon and Alouini, 2001], average bit error probability (ABEP) of TAG-QSM can be expressed as follows

$$ABEP \leq \frac{1}{\eta 2^\eta} \sum_{v=1}^{2^\eta} \sum_{a=1}^{2^\eta} P(\mathbf{x}_v \rightarrow \ \hat{\mathbf{x}}_a) e(\mathbf{x}_v, \hat{\mathbf{x}}_a). \tag{3.11}$$

where $P(\mathbf{x}_v \rightarrow \ \hat{\mathbf{x}}_a)$, $e(\mathbf{x}_v)$ are pairwise error probability (PEP) and the total number of erroneous bits, when $\mathbf{x}_v$ is transmitted and, $\hat{\mathbf{x}}_a$ is detected erroneously. The conditional pairwise error probability (CPEP) of TAG-QSM can be stated as

$$P(\mathbf{x}_v \rightarrow \ \hat{\mathbf{x}}_a | \mathbf{H}) = Q\left(\sqrt{\frac{\rho||\mathbf{H}(\mathbf{x}_v - \hat{\mathbf{x}}_a)||^2}{2}}\right). \tag{3.12}$$

CPEP can also be expressed as in (3.13) by using $Q(x) = \frac{1}{\pi}\int_0^{\frac{\pi}{2}} \exp(\frac{-x^2}{\sin^2\theta})\, dx$ equality.

$$P(\mathbf{x_v} \rightarrow \ \hat{\mathbf{x}}_a | \mathbf{H}) = \frac{1}{\pi}\int_0^{\frac{\pi}{2}} \exp\left(\frac{\rho||\mathbf{H}(\mathbf{x_v} - \hat{\mathbf{x}}_a)||^2}{4\sin^2\theta}\right) d\theta. \tag{3.13}$$

PEP can be stated as in (3.14) by taking the average of CPEP over **H** using moment generating function (MGF).

$$P(\mathbf{x}_v \to \hat{\mathbf{x}}_a) = \frac{1}{\pi}\int_0^{\frac{\pi}{2}} \left(\frac{\sin^2\theta}{\sin^2\theta + \frac{\rho||(\mathbf{x}_v - \hat{\mathbf{x}}_a)||^2}{4}} \right)^{N_R} d\theta. \tag{3.14}$$

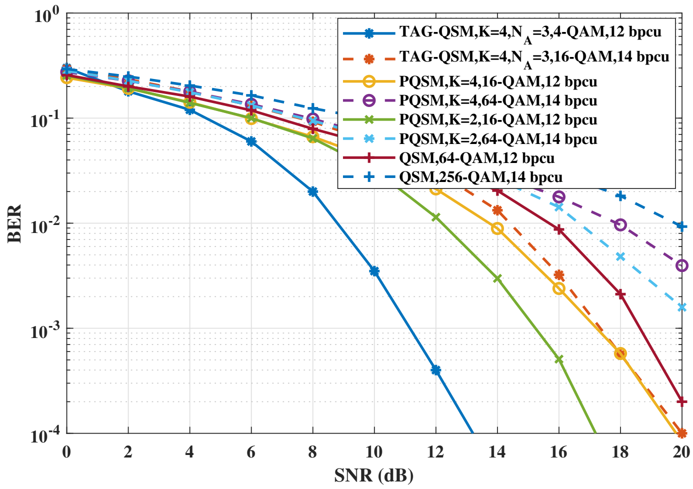

Figure 3.2: BER performance comparison of TAG-QSM ($K = 4$, $N_A = 2$) with the benchmark schemes for a 8×8 MIMO system under 12 and 14 bpcu.

3.3 Simulation Results

In this section, the BER performance comparison of TAG-QSM scheme is performed with the benchmark schemes PQSM [Huang et al., 2019] and classical QSM [Mesleh et al., 2014] by using Monte Carlo simulations. In addition, the BER performance of the TAG-QSM is compared with the theoretical upper bound which is derived in Section 3.2. Monte Carlo simulations are performed for at least 10^4 channel realizations.

In Fig. 3.2, TAG-QSM, QSM [Mesleh et al., 2014] and PQSM [Huang et al., 2019] schemes are compared for 8×8 MIMO system under 12 bpcu and 14 bpcu, respectively. For TAG-QSM scheme, simulations are performed for $K = 4$ and $N_A = 3$, while the simulations are demonstrated for $K = 2$ and $K = 4$. As seen

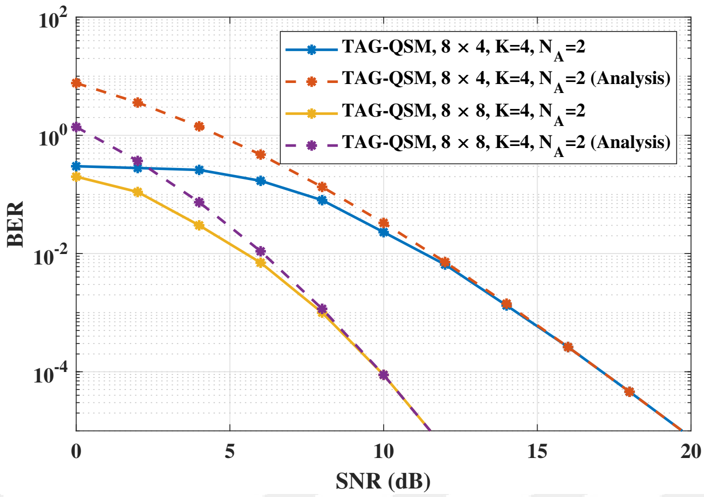

Figure 3.3: BER performance comparison of TAG-QSM ($K = 4$, $N_A = 2$) with the theoretical upper bound for a 8×8 and 8×4 MIMO systems under 10 bpcu.

in the Fig. 3.2, TAG-QSM outperforms the benchmark schemes at least 3 dB at the BER level of 10^{-3} under both data rates. The reason for this advantage is that TAG-QSM reduces modulation order by transmitting more bits with IM compared to the benchmark schemes.

In Figure 3.3, the theoretical BER upper bound expression of TAG-QSM scheme is compared with Monte Carlo simulations. The comparisons are performed for $K = 4$, $N_A = 2$, 4-QAM and 8×4 and 8×8 systems, respectively. As seen from the Fig. 3.3, the theoretical expression and computer simulations match at high SNR values.

Chapter 4

FLEXIBLE SPATIAL MODULATION WITH TRANSMIT ANTENNA SELECTION FOR MIMO SYSTEMS

In this chapter, flexible SM with transmit antenna selection (FSM-TAS) is proposed for MIMO systems. The contributions of this novel FSM-TAS scheme is stated as follows. The number of active antennas is not fixed and it is determined by incoming bits. In this way, additional bits can carry information and transmit antennas can be used in a flexible way. These advantages become more clear when the number of transmit antennas increases since the number of additional bits and the upper limit of active transmit antennas increases in this case. After the number of active antennas is decided, the active antennas are determined using norm based sortation to increase SNR. In this way, all possible channel combinations do not need to be considered and this decreases transmitter complexity. After the system model of FSM-TAS is introduced, complexity analysis and outage probability derivations are expressed. Then, Monte Carlo simulations are performed to compare FSM-TAS and ESM-GAS [Qing et al., 2021] at the same spectral efficiency, to assess the potential of FSM-TAS with different number of selected channel combination values. Besides, theoretical expressions and Monte Carlo simulations for the outage probability are compared for validation.

4.1 System Model

We consider a MIMO system with N_T transmit antennas, N_R receive antennas and M-ary constellation. The channel between transmitter and receiver follows Rayleigh fading and denoted as $\mathbf{H} \in \mathbb{C}^{N_R \times N_T}$, where $h_{i,j}$ with $i \in \{1, 2, ..., N_R\}$ and $j \in \{1, 2, ..., N_T\}$ represents channel gain between i-th receive and j-th transmit antennas, which is assumed to be an independent and identically distributed complex

Gaussian random variable with $\mathcal{CN}(0,1)$ distribution. It is also assumed that both transmitter and receiver have perfect CSI (PCSI).

4.1.1 Transmitter Side

The vector of channel coefficients between the k-th transmit and all receive antennas can be expressed as $\mathbf{h}_k = [h_{1,k}, h_{2,k}, ..., h_{N_R,k}]^T$. N_A is the number of active antennas out of N_T transmit antennas and varies as $1 \leq N_A \leq N_T/2$ with respect to incoming bits,the number of possible transmit antenna combinations can be shown as $K = \binom{N_T}{N_A}$, where $\binom{a}{b} = \frac{a!}{(a-b)!b!}$ is the binomial coefficient. The combination set, which includes all possible channel combinations with N_A active antennas, can be shown as $Q_{N_A} = \{\hat{\mathbf{h}}_{1,N_A},\hat{\mathbf{h}}_{2,N_A},\hat{\mathbf{h}}_{3,N_A},...\hat{\mathbf{h}}_{K,N_A}\}$ and the construction of n-th element of Q_{N_A} is shown as in (4.1), where $\mathbf{h}_{t_{n,m}}$ is the channel coefficient vector of $t_{n,m}$-th transmit antenna and $t_{n,m}$ is the index of m-th active antenna of n-th element in Q_{N_A} for $t_{n,m} \in \{1, 2, ..., N_T\}$, $n \in \{1, 2, .., K\}$, $m \in \{1, 2, .., N_A\}$:

$$\hat{\mathbf{h}}_{n,N_A} = \frac{1}{\sqrt{N_A}} \sum_{m=1}^{N_A} \mathbf{h}_{t_{n,m}}. \tag{4.1}$$

In the FSM-TAS system model, the incoming bits that are accepted by the transmitter are divided into 3 main subgroups as $\mathbf{b}_1$, $\mathbf{b}_2$ and $\mathbf{b}_3$. Using b_1 bit group, N_A is determined and a sample mapping for N_A with $N_T = 8$ can be seen in Table I. After N_A is determined, Q_{N_A} is constructed by following (4.1) and the combinations of channel coefficients are sorted with respect to their gains as in (4.2), where $\tilde{\mathbf{h}}_{r,N_A}$ has the r-th largest gain:

$$\left\|\hat{\mathbf{h}}_{1,N_A}\right\|^2 > \left\|\tilde{\mathbf{h}}_{2,N_A}\right\|^2 > \left\|\tilde{\mathbf{h}}_{3,N_A}\right\|^2 > ... > \left\|\tilde{\mathbf{h}}_{K,N_A}\right\|^2. \tag{4.2}$$

Then, S out of K transmit antenna combinations with largest gains from (4.2) are selected to apply SM, where S is assumed to be an integer power of two. The selected combinations are mapped into $\mathbf{b}_2$ and one combination for the transmission of data symbol is determined. A sample mapping of the selected combinations over $\mathbf{b}_2$ with $N_T = 8$, $S = 4$, $N_A = 2$ can be seen in Table II. The determined combination of channel coefficients is shown as $\tilde{\mathbf{h}}_{f,N_A}$, where f is the index of determined combination $f \in \{1, 2, ..., S\}$. Besides, $\tilde{t}_{f,g}$ represents the index of the g-th active transmit

Table 4.1: Mapping for N_A with $N_T = 8$

$\mathbf{b}_1$	N_A
00	1
01	2
10	3
11	4

Table 4.2: Mapping for selected channel combinations with $N_T = 8$, $N_A = 2$ and $S = 4$

$\mathbf{b}_2$	Selected combination	Channel coefficients
00	$\tilde{h}_{1,2}$	h_1,h_2
01	$\tilde{h}_{2,2}$	h_4,h_6
10	$\tilde{h}_{3,2}$	h_3,h_7
11	$\tilde{h}_{4,2}$	h_1,h_8

antenna of determined combination, where $g \in \{1, 2, ..., N_A\}$. The last bit group $\mathbf{b}_3$ determines data symbol, s, and the same symbol is transmitted over all active antennas in each time slot. In this way, FSM-TAS requires just a single RF chain independent from N_A since all activated antennas transmit the same data symbol. The lengths of $\mathbf{b}_1$, $\mathbf{b}_2$, $\mathbf{b}_3$ are $\log_2(\frac{N_T}{2})$, $\log_2 S$, $\log_2 M$, respectively, and the spectral efficiency of the FSM-TAS in bits per channel use (bpcu) can be expressed as

$$\eta = \log_2(\frac{N_T}{2}) + \log_2 S + \log_2 M. \tag{4.3}$$

After the number of active antennas, the indices of active antennas and data symbol are determined, the transmit vector $\mathbf{x} \in \mathbb{C}^{N_T \text{x} 1}$ is created as

$$\mathbf{x} = \frac{1}{\sqrt{N_A}}[0, 0, \underbrace{s}_{\tilde{t}_{f,1}}, 0, \underbrace{s}_{\tilde{t}_{f,2}}, ..., \underbrace{s}_{\tilde{t}_{f,N_A}}, 0, 0]^T \tag{4.4}$$

where $E[\mathbf{x}^H \mathbf{x}] = 1$. An example is shown below for transmission process of the proposed FSM-TAS scheme with $N_T = 8$, $S = 4$.

Example: Assume that $N_T = 8$ and N_A changes as $1 \leq N_A \leq 4$ with respect to incoming bits. Then, $S = 4$ of K possible combinations are selected to apply SM. In case of 4-QAM, the spectral efficiency is obtained as 6 bpcu. Assume that incoming bits are [011011], and these are separated into subgroups as $\mathbf{b}_1 = [01]$, $\mathbf{b}_2 = [10]$, $\mathbf{b}_3 = [11]$. By looking at Table 4.1, it can be seen that $\mathbf{b}_1 = [01]$ determines the number of active antennas as $N_A = 2$. $\mathbf{b}_2 = [10]$ determines $\tilde{\mathbf{h}}_{f,N_A} = \tilde{\mathbf{h}}_{3,2}$ which can be seen from Table 4.2 and it is clear that the indices of activated antennas will be $\tilde{t}_{3,1} = 3$, $\tilde{t}_{3,2} = 7$. The last bit group $\mathbf{b}_3 = [11]$ decides data symbol as $s = 0.7 - 0.7i$. After the indices of activated antennas and data symbol are determined, the transmit vector is obtained as $\mathbf{x} = \frac{1}{\sqrt{2}}[0, 0, \underbrace{0.7 - 0.7i}_{\tilde{t}_{3,1}=3}, 0, 0, 0, \underbrace{0.7 - 0.7i}_{\tilde{t}_{3,2}=7}, 0]^T$.

4.1.2 Receiver Side

The received signal $\mathbf{y} \in \mathbb{C}^{N_R \text{x} 1}$ at the receiver side is given in (4.5), where $\mathbf{n} \in \mathbb{C}^{N_R \text{x} 1}$ is additive white Gaussian noise vector with $\mathcal{CN}(0, 1)$, and ρ is average signal to noise ratio at each receiver antenna:

$$\mathbf{y} = \sqrt{\rho}\tilde{\mathbf{h}}_{f,N_A} s + \mathbf{n}, \tag{4.5}$$

N_A, the selected combination and data symbol are determined using maximum likelihood (ML) detector at the receiver. This detector works as follows

$$[\hat{N}_A, \hat{f}, \hat{s}] = \underset{N_A, f, s}{\arg\min} ||\mathbf{y} - \sqrt{\rho}\tilde{\mathbf{h}}_{f,N_A} s||^2. \tag{4.6}$$

In (4.6), $\hat{N}_A$, $\hat{f}$ and $\hat{s}$ stand for the detected number of active antennas, the index of channel combination and data symbol, respectively.

4.2 Complexity Analysis

In this section, the average transmitter and receiver complexities of the proposed FSM-TAS scheme are calculated separately. In [Rajashekar et al., 2013], the transmitter complexity of COAS scheme is defined as the required number of complex multiplications and additions to order the norm squares of channel vectors. By following the same procedure, the transmitter complexity of FSM-TAS scheme, which

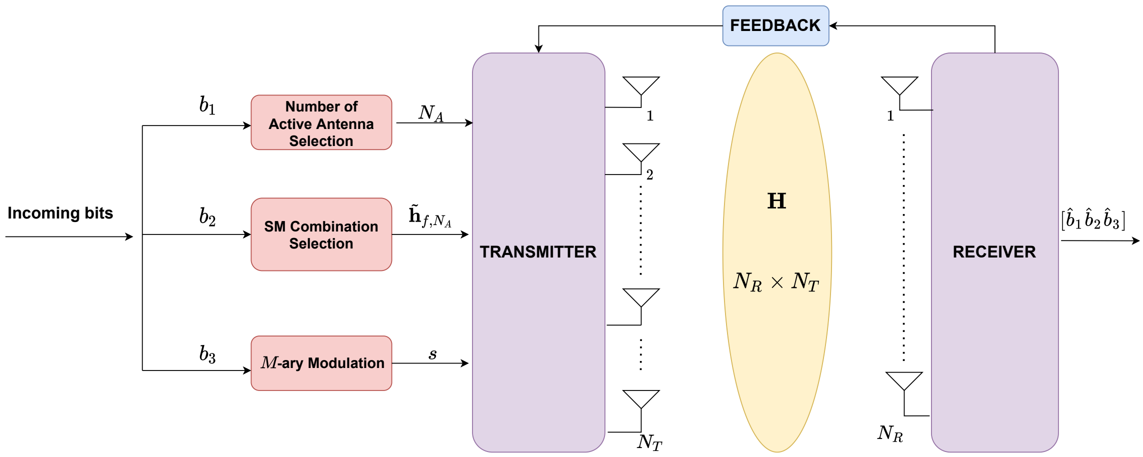

Figure 4.1: FSM-TAS System Model.

is the required number of complex additions (CAs) and complex multiplications (CMs) to order the norm squares of the combinations of channel coefficients as in (4.2) for determined N_A, is calculated.As mentioned before, N_A varies between 1 and $N_T/2$ with equal probability and the average transmitter complexity of FSM-TAS scheme can be calculated as

$$C_{\text{Tx,FSM-TAS}} = \frac{\sum_{N_A=1}^{N_T/2} \binom{N_T}{N_A}[(N_A+2)N_R - 1]}{N_T/2}. \tag{4.7}$$

On the other hand, the benchmark ESM-GAS scheme sorts all possible combinations of channel coefficients. Then, transmitter complexity of ESM-GAS is given as

$$C_{\text{Tx,ESM-GAS}} = \sum_{N_A=1}^{N_T} \binom{N_T}{N_A}[(N_A+2)N_R - 1]. \tag{4.8}$$

Since ESM-GAS compares all possible combinations of channel coefficients in each time slot, proposed FSM-TAS scheme has lower average transmitter complexity than ESM-GAS as can be seen from (4.7) and (4.8).

In the next step, the average receiver complexity of FSM-TAS scheme is calculated. The average receiver complexity is measured by the total number of CAs and CMs that is required to make the detection in (4.6). Then, the average of required number of complex calculations for FSM-TAS is,

$$C_{\text{Rx,FSM-TAS}} = ((3\frac{(\frac{N_T}{2}+1)}{2} + 2)N_R - 1)2^{\eta}, \tag{4.9}$$

where $(\frac{\frac{N_T}{2}+1}{2})$ is the expected value of N_A in FSM-TAS. Different than the FSM-TAS scheme, N_A changes between 1 and N_T in ESM-GAS and the expected value of N_A in ESM-GAS is $(\frac{N_T+1}{2})$. The average receiver complexity for ESM-GAS can be calculated as

$$C_{\text{Rx,ESM-GAS}} = ((3(\frac{N_T+1}{2}) + 2)N_R - 1)2^{\eta'}, \tag{4.10}$$

where η' is the spectral efficiency of the ESM-GAS scheme. For a fair comparison, under the same spectral efficiency (i.e, $\eta = \eta'$), (4.9) and (4.10) show that FSM-TAS scheme has lower average receiver complexity than ESM-GAS. This is caused by the difference in possible values of N_A in these schemes. For instance, for $N_T = 8$, $N_R = 2$, FSM-TAS has 86% lower transmitter and 41% lower receiver complexity, respectively.

4.3 Outage Probability

In this section, the outage probability analysis of FSM-TAS is performed. In [Proakis, 2000], $||\mathbf{h}_k||^2$ is given as a chi-squared random variable with $2N_R$ degrees of freedom. Adding the channel vectors linearly as in (4.1) to get the combinations does not effect the degrees of freedom and $||\hat{\mathbf{h}}_{n,N_A}||^2$ is also a chi-squared random variable with $2N_R$ degrees of freedom. The pdf and cdf of $||\hat{\mathbf{h}}_{n,N_A}||^2$ are shown in (4.11) and (4.12) respectively:

$$f_{||\hat{\mathbf{h}}_{n,N_A}||^2}(x) = \frac{x^{N_R-1}e^{-x}}{\Gamma(N_R)}, \tag{4.11}$$

$$F_{||\hat{\mathbf{h}}_{n,N_A}||^2}(x) = 1 - e^{-x}\sum_{i=0}^{N_R-1}\frac{x^i}{i!} = \frac{\gamma(N_R,x)}{\Gamma(N_R)}. \tag{4.12}$$

Here, $\Gamma(.)$, $\gamma(.,.)$ and $\beta(.,.)$ are the upper incomplete gamma function, the lower incomplete gamma function and beta function respectively. As mentioned above, S out of K combinations of channel coefficients with maximum norm squares are selected to apply SM in FSM-TAS scheme. After sorting the combinations as in (4.2), in [David and Nagaraja, 2004], the pdf of $||\tilde{\mathbf{h}}_{S,N_A}||^2$ is given as

$$\begin{aligned} f_{||\tilde{\mathbf{h}}_{S,N_A}||^2}(x) =& \frac{1}{\beta(K-S+1,S)}\{F_{||\hat{\mathbf{h}}_{n,N_A}||^2}(x)\}^{(K-S)} \\ & \times\{1 - F_{||\hat{\mathbf{h}}_{n,N_A}||^2}(x)\}^{(S-1)} f_{||\hat{\mathbf{h}}_{n,N_A}||^2}(x), \end{aligned} \tag{4.13}$$

Then, the pdf of instantaneous received SNR (γ_i) for the determined N_A can be expressed as in (4.14)

$$\begin{aligned} f_{\gamma_i}^{N_A}(x) = \frac{1}{S}\sum_{l=1}^{S} \frac{1}{\beta(K-l+1,l)}\{F_{||\hat{\mathbf{h}}_{n,N_A}||^2}(x)\}^{(K-l)} \\ \times\{1 - F_{||\hat{\mathbf{h}}_{n,N_A}||^2}(x)\}^{(l-1)} f_{||\hat{\mathbf{h}}_{n,N_A}||^2}(x), \end{aligned} \tag{4.14}$$

For the determined N_A, the outage probability of FSM-TAS scheme is defined as $P_{out,N_A}(\gamma, R) = P\{\gamma_i < \gamma_{th}\} = \int_0^{\gamma_{th}} f_{\gamma_i}^{N_A}(x)\,dx$, where R is the predetermined spectral efficiency, γ is the average SNR and $\gamma_{th} = \frac{2^R-1}{\gamma}$ is the threshold SNR value.

After inserting (4.11), (4.12), (4.13) and (4.14) into the outage probability expression, the outage probability of FSM-TAS can be expressed as

$$\begin{aligned} P_{out,N_A}(\gamma, R) = & \frac{1}{\Gamma(N_R)S}\sum_{l=1}^{S}\frac{1}{\beta(K-l+1,l)}\int_0^{\gamma_{th}} x^{N_R-1}e^{-x} \\ & \times\{\frac{\gamma(N_R,x)}{\Gamma(N_R)}\}^{(K-l)}\{1-\frac{\gamma(N_R,x)}{\Gamma(N_R)}\}^{(l-1)}\,dx. \end{aligned} \tag{4.15}$$

Since N_A changes with respect to incoming bits, the average outage probability is calculated and expressed as

$$P_{out,avg}(\gamma, R) = \frac{1}{N_T/2}\sum_{N_A=1}^{N_T/2} P_{out,N_A}(\gamma, R). \tag{4.16}$$

4.4 Simulation results

In this section, Monte Carlo simulations are performed to test the BER performance of FSM-TAS for different S values and to compare the BER performances of FSM-TAS and ESM-GAS [Qing et al., 2021] under the same spectral efficiency for a fair comparison. In addition, a comparison is performed between the theoretical outage probability expression in Section 4.3 and Monte Carlo simulations. Simulations are performed for a MIMO system with $N_T = 8$ and different N_R values.

Fig. 4.2(a) shows BER performances of FSM-TAS for $S = 2$, $S = 4$ and $S = 8$ at $\eta = 8$ bpcu spectral efficiency. BER performance decreases when S increases despite the modulation order also decreases. The reason is that decreasing S means

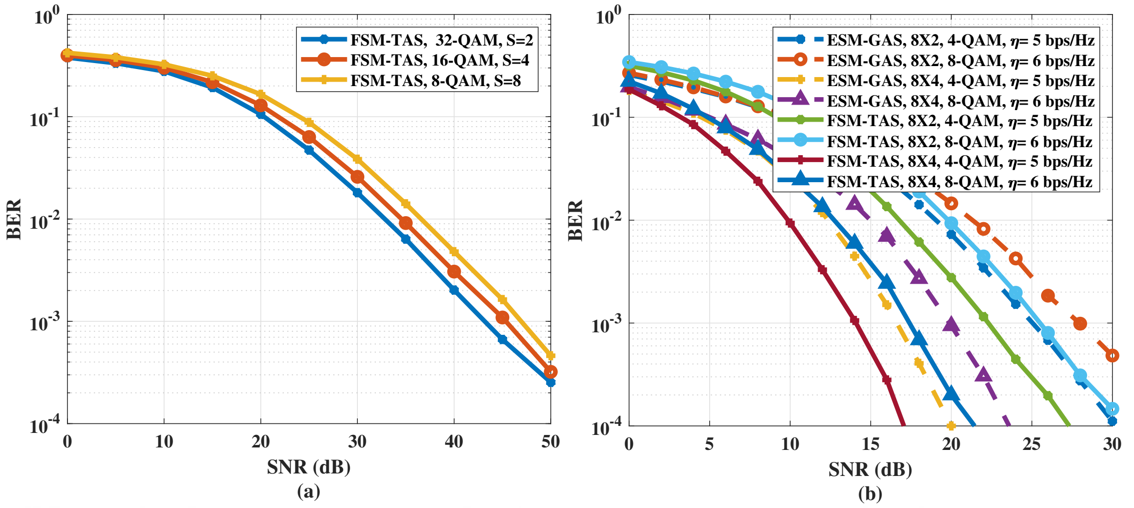

Figure 4.2: BER performances of (a) FSM-TAS for $S = 2$, $S = 4$, $S = 8$ at $\eta = 8$ bitpcu with 8×1 MIMO system, (b) FSM-TAS for $S = 2$ and ESM-GAS under $\eta = 5$, 6 bpcu with 8×2 and 8×4 MIMO systems.

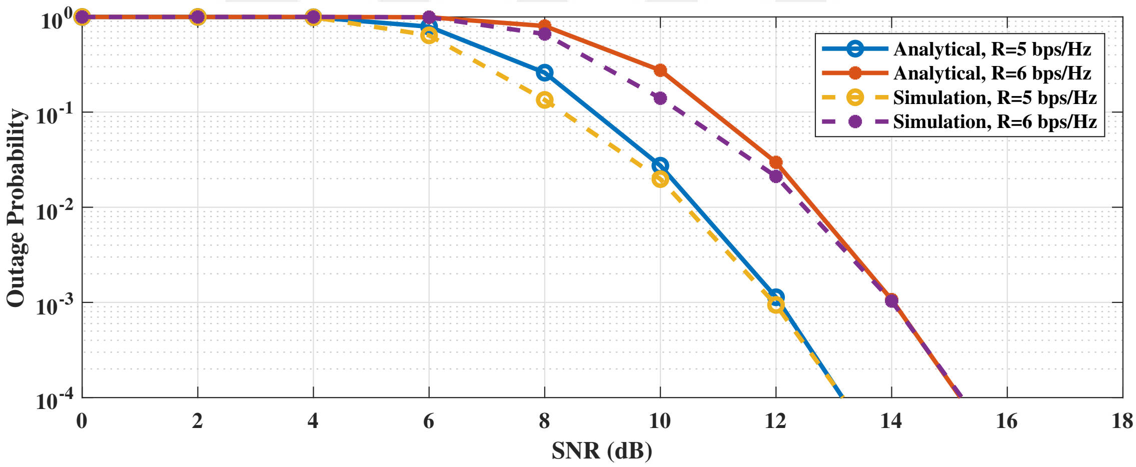

Figure 4.3: Theoretical expression and Monte Carlo simulation results for outage probability of FSM-TAS at $\eta = 5$ and 6 bpcu with $N_T = 8$, $N_R = 1$.

to have less but more powerful combinations of channel coefficients and it enhances the BER performance of the system despite using a higher modulation order. A BER comparison between the proposed FSM-TAS scheme and ESM-GAS is shown in Fig. 4.2(b) under $\eta = 5$, 6 bpcu. As seen from Fig. 4.2(b), FSM-TAS with $S = 2$ has approximately 3 dB gain at 10^{-4} with respect to ESM-GAS under the same spectral efficiency since FSM-TAS carries additional bits to determine N_A and selects less and more powerful combinations with respect to ESM-GAS. In Fig. 4.3, the theoretical outage probability results derived in Section 4.3 is compared with simulation results. We see that theoretical derivations and simulation results are in agreement at high SNR values and they are close to each other at low SNR values.

Chapter 5

SPATIAL MODULATION USING SIGNAL SPACE DIVERSITY

In this chapter, the novel transmission scheme named SM using signal space diversity (SM-SSD) is proposed for MIMO systems. The proposed SM-SSD scheme modulate T time slots simultaneously, uses SSD and cleverly creates transmission vectors to enhance diversity order and bit error rate (BER) performance. The antenna activation pattern (AAP) determination and time activation pattern (TAP) algorithms are presented to determine the transmission order of data symbols and active antenna indices in each time slot, respectively. It is shown that the proposed scheme enhances transmit diversity and has better BER performance than existing schemes in the literature. In addition to this, SM-SSD requires only one radio frequency (RF) chain, which is the main advantage of classical SM. After the system model of SM-SSD is introduced, the theoretical upper bound of BER is derived. Besides, Monte Carlo simulations are performed to compare the BER performance of SM-SSD with the existing schemes in the literature and show that enhanced transmit diversity improves the BER performance of SM-SSD considerably. In addition, Monte Carlo simulations are also performed to check the validity of theoretical upper bound derivations and observe the effect of correlated channel coefficients between transmitter and receiver.

5.1 System Model

We consider a MIMO configuration with N_t transmit and N_r receive antennas. A total number of b bits are transmitted over T successive time slots and these bits are split into four parts. Firstly, $b_1 = T\log_2(M)$ bits determine T M-PSK/QAM modulated data symbols, $\mathbf{s} = [s_1, s_2, \cdots, s_T]^{\mathrm{T}}$, where M and $(\cdot)^{\mathrm{T}}$ are the modulation

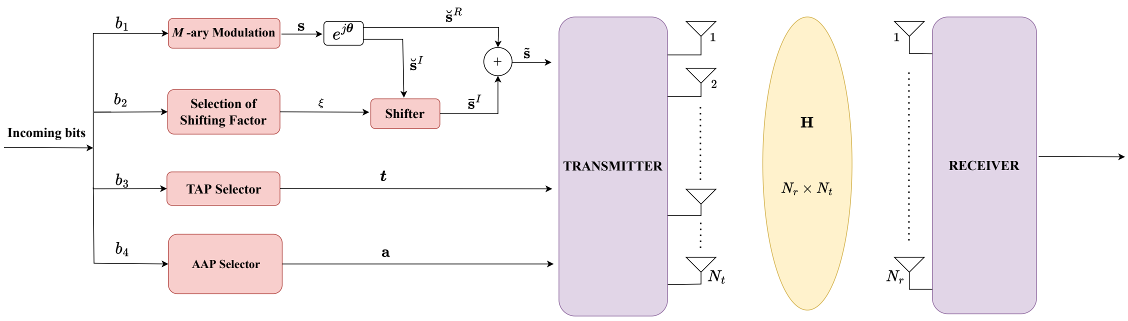

Figure 5.1: SM-SSD System Model.

order and transposition operator, respectively. The μ-th element of the data symbol vector is rotated with an angle θ_μ, $\breve{\mathbf{s}} = [s_1 e^{j\theta_1}, s_2 e^{j\theta_2}, \cdots, s_T e^{j\theta_T}]^{\mathrm{T}}$, $\mu = 1, \cdots, T$, and this rotated data symbol vector is separated into its real and imaginary parts as $\breve{\mathbf{s}}^R$ and $\breve{\mathbf{s}}^I$, where $\breve{\mathbf{s}} = \breve{\mathbf{s}}^R + j\breve{\mathbf{s}}^I$. Note that constellation rotation is a must in SSD-based schemes to provide a diversity gain [Boutros and Viterbo, 1998]. Secondly, in order to apply SSD, $b_2 = \lfloor \log_2(T-1) \rfloor$ bits decide a shifting factor ξ to shift the vector $\breve{\mathbf{s}}^I$ circularly and its circularly shifted version is expressed as $\bar{\mathbf{s}}^I = [\bar{s}_1^I, \bar{s}_2^I, \cdots, \bar{s}_T^I]^{\mathrm{T}}$, where $\bar{\mathbf{s}}_k^I = \breve{\mathbf{s}}_i^I$, $\xi \in \{1, \cdots, T-1\}$, $k = \mathrm{mod}(i-\xi, T)$ if $\mathrm{mod}(i-\xi, T) > 0$ and $k = T$ if $\mathrm{mod}(i-\xi, T) = 0$, $i, k \in \{1, \cdots, T\}$. Then, the new data symbol vector is obtained as $\tilde{\mathbf{s}} = \breve{\mathbf{s}}^R + j\bar{\mathbf{s}}^I = [\tilde{s}_1, \tilde{s}_2, \cdots, \tilde{s}_T]^{\mathrm{T}}$. Hence, the real and imaginary parts of each data symbol are transmitted over different time slots. Thirdly, $b_3 = \lfloor \log_2(T!) \rfloor$ bits select the time slot activation pattern (TAP), $\mathbf{t} = [t_1, t_2, \cdots, t_T]^{\mathrm{T}}$, $t_\mu \in \{1, 2, \cdots, T\}$. Fourthly, $b_4 = \log_2(N_t)$ bits specify the antenna activation pattern (AAP), $\mathbf{a} = [a_1, a_2, \cdots, a_T]^{\mathrm{T}}$. The method for the generation of TAPs and AAPs is discussed in the sequel. Finally, the μ-th data symbol ($\tilde{\mathbf{s}}_\mu$) is transmitted in time slot t_μ from the a_μ-th transmit antenna. The transmitted vector $\mathbf{x}^{(t_\mu)} \in \mathbb{C}^{N_t \times 1}$ at time slot t_μ can be shown as:

$$\mathbf{x}^{(t_\mu)} = [0, \cdots, \underbrace{\tilde{s}_\mu}_{a_\mu}, \cdots, 0]^{\mathrm{T}}. \tag{5.1}$$

Therefore, the transmission matrix is given as $\mathbf{X} = [\mathbf{x}^{(1)}, \cdots, \mathbf{x}^{(T)}] \in \mathbb{C}^{N_t \times T}$, whose t_μ-th column represents $\mathbf{x}^{(t_\mu)}$. The spectral efficiency of the proposed scheme in bits

Table 5.1: Shifting Mechanism of $\breve{\mathbf{s}}^I$ According to b_2 Bits for $T = 3$.

b_2 bits	ξ	$\bar{\mathbf{s}}^I$
$\{0\}$	1	$[\breve{s}_3^I \breve{s}_1^I \breve{s}_2^I]^{\mathrm{T}}$
$\{1\}$	2	$[\breve{s}_2^I \breve{s}_3^I \breve{s}_1^I]^{\mathrm{T}}$

Table 5.2: TAP Selection According to b_3 Bits for $T = 3$.

b_3 bits	TAP ($\mathbf{t}$)
$\{00\}$	$[1, 2, 3]^{\mathrm{T}}$
$\{01\}$	$[1, 3, 2]^{\mathrm{T}}$
$\{10\}$	$[2, 1, 3]^{\mathrm{T}}$
$\{11\}$	$[2, 3, 1]^{\mathrm{T}}$

per channel use (bpcu) can be given as:

$$\eta = \frac{T \log_2(M) + \lfloor \log_2(T-1) \rfloor + \lfloor \log_2(T!) \rfloor + \lfloor \log_2(N_t) \rfloor}{T}. \tag{5.2}$$

Remark 1 (TAPs Creation): Since the length of a TAP is T, a total number of all possible TAPs is $T!$ by permutation. Thus, the set, which includes all possible TAPs, is given as $\mathcal{T} = \{\mathbf{t}_1, \cdots, \mathbf{t}_{T!}\}$, $\mathbf{t}_g = [t_{g,1}, \cdots, t_{g,T}]^{\mathrm{T}}$, $g = 1, \cdots, T!$. For example, assuming $T = 3$, the set is expressed as follows:

$$\mathcal{T} = \left\{ \begin{bmatrix} 1 \\ 2 \\ 3 \end{bmatrix}, \begin{bmatrix} 1 \\ 3 \\ 2 \end{bmatrix}, \begin{bmatrix} 2 \\ 1 \\ 3 \end{bmatrix}, \begin{bmatrix} 2 \\ 3 \\ 1 \end{bmatrix}, \begin{bmatrix} 3 \\ 1 \\ 2 \end{bmatrix}, \begin{bmatrix} 3 \\ 2 \\ 1 \end{bmatrix} \right\}. \tag{5.3}$$

Only $2^{\lfloor \log_2(T!) \rfloor}$ out of $T!$ possible TAPs can be utilized to transmit $\lfloor \log_2(T!) \rfloor$ number of information bits by the indices of TAPs. In this study, we employ the first $2^{\lfloor \log_2(T!) \rfloor}$ TAPs.

Remark 2 (AAPs Creation): Here, we propose a clever AAP selection strategy. Let's define a set $\mathcal{A} = \{\mathbf{a}_1, \cdots, \mathbf{a}_{N_t}\}$, which includes all possible AAPs. The ν-th

AAP is defined as follows:

$$\mathbf{a}_\nu = [\mathrm{mod}(\nu, N_t), \mathrm{mod}(\nu+1, N_t), \cdots, \mathrm{mod}(\nu+T-1, N_t)]^{\mathrm{T}}. \tag{5.4}$$

If any element of $\mathbf{a}_\nu$ is equal to 0, its value is changed as N_t. For instance, assuming $N_t = 4$ and $T = 3$, the set including all possible AAPs is given by

$$\mathcal{A} = \left\{ \begin{bmatrix} 1 \\ 2 \\ 3 \end{bmatrix}, \begin{bmatrix} 2 \\ 3 \\ 4 \end{bmatrix}, \begin{bmatrix} 3 \\ 4 \\ 1 \end{bmatrix}, \begin{bmatrix} 4 \\ 1 \\ 2 \end{bmatrix} \right\}. \tag{5.5}$$

The received signal $\mathbf{y} \in \mathbb{C}^{N_R \mathrm{x} 1}$ at the receiver side is given by

$$\mathbf{y} = \sqrt{\rho}\mathbf{H}\mathbf{x} + \mathbf{n} \tag{5.6}$$

where $\mathbf{H} \in \mathbb{C}^{N_r \mathrm{x} N_t}$ is a Rayleigh fading channel matrix whose entries independent and identically distributed complex Gaussian random variables with $\mathcal{CN}(0,1)$ distribution and $\mathbf{n} \in \mathbb{C}^{N_t \mathrm{x} 1}$ is an additive white Gaussian noise vector whose entries are independent and identically distributed complex Gaussian random variables with $\mathcal{CN}(0,1)$. ρ is average signal-to-noise ratio at each receiver antenna. At the receiver, indices of activated transmit antennas and data symbols are determined using maximum likelihood (ML) detector. ML detector is applied for T consecutive time slots and it works as follows

$$[\hat{\xi}, \hat{\mathbf{a}}, \hat{\mathbf{t}}, \hat{\mathbf{s}}] = \underset{\xi, \mathbf{a}, \mathbf{t}, \mathbf{s}}{\arg\min} \sum_{n=1}^{T} ||\mathbf{y}^{(n)} - \sqrt{\rho}\mathbf{H}^{(n)}\mathbf{x}^{(n)}||^2, \tag{5.7}$$

where $\mathbf{y}^{(n)}$, $\mathbf{H}^{(n)}$ are the received signal vector and the channel matrix for the corresponding n-th time slot, respectively. In (5.7), $\hat{\xi}$,$\hat{\mathbf{a}}$, $\hat{\mathbf{t}}$ and $\hat{\mathbf{s}}$ stand for the detected shifting factor, AAP, TAP and the data symbol vector, respectively. Here, an ML detector makes an exhaustive search over all possible transmission matrices, thus, the number of ML metric calculations in (5.7) is $T\eta$. For constant T and M, the decoding complexity increases linearly with N_t as in SM.

5.2 *Performance Analysis and BER Optimization*

In this section, the theoretical analysis of the BER performance of SM-SSD, and optimization of its rotation angles are presented. In addition, a diversity analysis and correlated channels are discussed.

5.2.1 Theoretical Analysis and Optimization

In this subsection, firstly, we obtain an upper bound on the BER of SM-SSD system under the assumption of ML detection. As in [Simon and Alouini, 2001], an upper bound on the BER of SM-SSD can be obtained as:

$$P_b \leq \frac{1}{(T\eta)2^{(T\eta)}} \sum_{\omega=1}^{2^{(T\eta)}} \sum_{a=1}^{2^{(T\eta)}} P(\mathbf{X}_\omega \rightarrow \hat{\mathbf{X}}_\phi) e(\mathbf{X}_\omega, \hat{\mathbf{X}}_\phi). \tag{5.8}$$

In (5.8), $P(\mathbf{X}_\omega \rightarrow \hat{\mathbf{X}}_\phi)$ and $e(\mathbf{X}_\omega, \hat{\mathbf{X}}_\phi)$ are pairwise error probability (PEP) and the number of erroneous bits, respectively, when $\mathbf{X}_\omega$ is transmitted and $\hat{\mathbf{X}}_\phi$ is incorrectly detected. For the proposed scheme, the conditional pairwise error probability (CPEP) can be expressed as follows

$$P(\mathbf{X}_\omega \rightarrow \hat{\mathbf{X}}_\phi | \mathbf{H}) = Q\left(\sqrt{\frac{\rho||\mathbf{H}(\mathbf{X}_\omega - \hat{\mathbf{X}}_\phi)||^2}{2}}\right). \tag{5.9}$$

where $Q(x) = \frac{1}{\pi}\int_0^{\frac{\pi}{2}} \exp(\frac{-x^2}{\sin^2\theta})\, d\theta$. PEP can be expressed as in (5.10) by taking the average of CPEP over $\mathbf{H}$ using moment generating function (MGF):

$$P(\mathbf{X}_\omega \rightarrow \hat{\mathbf{X}}_\phi) = \frac{1}{\pi}\int_0^{\frac{\pi}{2}} \kappa^{(1)}(\gamma)\kappa^{(2)}(\gamma)...\kappa^{(T)}(\gamma) d\gamma. \tag{5.10}$$

where $\kappa^{(\chi)}(\gamma) = \left(\frac{\sin^2\gamma}{\sin^2\gamma + \frac{\rho\lambda_\chi}{4}}\right)^{N_r}$, and $\lambda_\chi, \chi = 1, 2, ..., T$ are the eigenvalues of $(\mathbf{X}_\omega - \hat{\mathbf{X}}_\phi)^H(\mathbf{X}_\omega - \hat{\mathbf{X}}_\phi)$.

The BER performance of SM-SSD are dictated by the rotation vector $\boldsymbol{\theta}$. An exhaustive search for all elements of $\boldsymbol{\theta}$ is not efficient and due to this, we propose a suboptimal solution and define the elements of $\boldsymbol{\theta}$ depending on θ'. The μ-th element of $\boldsymbol{\theta}$ can be obtained as $\theta_\mu = \theta' + 90(\mu - 1)/T$. To determine the optimal θ' value, the minimum coding gain distance (MCGD) is considered. MCGD is calculated as follows

$$\delta_{\min} = \min_{\mathbf{X},\hat{\mathbf{X}}} \prod_{\chi=1}^{T} \lambda_{\chi}. \tag{5.11}$$

The optimal θ' can be expressed as below in the context of $\delta_{\min}$:

$$(\theta'_{\text{opt}}) = \arg\max_{\theta'} \delta_{\min}. \tag{5.12}$$

The maximum MCGD values are observed at $\theta'_{opt} = 11^o$ and $\theta'_{opt} = 18^o$ for 4-QAM and 8-QAM, respectively. Then, $\theta'_{opt} = 11^o$ and $\theta'_{opt} = 18^o$ are selected as suboptimal rotation angles for 4-QAM and 8-QAM, respectively.

To observe the effect of correlation between the channels, the Kronecker model is considered [Paulraj et al., 2003]. Accordingly, the correlated channel matrix can be expressed as $\mathbf{H}_{corr} = \mathbf{R}_L^{1/2}\mathbf{H}\mathbf{R}_R^{1/2}$ where $\mathbf{R}_L^{1/2} \in \mathbb{C}^{N_r \text{x} N_r}$ and $\mathbf{R}_R^{1/2} \in \mathbb{C}^{N_t \text{x} N_t}$ are spatial correlation matrices at the transmitter and the receiver, respectively. The entries of the spatial correlation matrices are $\mathbf{R}_{L,i,j}^{1/2} = \mathbf{R}_{R,i,j}^{1/2} = \tau^{-|i-j|}$ where τ is the correlation coefficient.

5.2.2 Diversity Analysis

In this section, we investigate the worst case pairwise error events to give insight on the diversity order of the proposed scheme.

Symbol Selection: We first investigate the effect of data symbol selection on the diversity order. Assume that the transmission matrix $\mathbf{X}$, with parameters $N_t = 4$, $T = 3$, $\xi = 1$, $\mathbf{t} = [1,3,2]^{\text{T}}$, $\mathbf{a} = [2,3,4]^{\text{T}}$, $\breve{\mathbf{s}} = [\breve{s}_1, \breve{s}_2, \breve{s}_3]^{\text{T}}$, is transmitted, and $\hat{\mathbf{X}}$ is erroneously detected only with a single symbol error ($\breve{s}_1 \rightarrow \breve{s}_{e,1}$) while shifting factor, TAP, and AAP are decoded correctly. In this case, the corresponding error event can be expressed as follows:

$$\mathbf{X} \rightarrow \hat{\mathbf{X}} = \begin{bmatrix} 0 & 0 & 0 \\ \breve{s}_1^R + j\breve{s}_3^I & 0 & 0 \\ 0 & \breve{s}_3^R + j\breve{s}_2^I & 0 \\ 0 & 0 & \breve{s}_2^R + j\breve{s}_1^I \end{bmatrix} \rightarrow \begin{bmatrix} 0 & 0 & 0 \\ \breve{s}_{e,1}^R + j\breve{s}_3^I & 0 & 0 \\ 0 & \breve{s}_3^R + j\breve{s}_2^I & 0 \\ 0 & 0 & \breve{s}_2^R + j\breve{s}_{e,1}^I \end{bmatrix}. \tag{5.13}$$

For this specific error event, $\mathbf{A} = (\mathbf{X} - \hat{\mathbf{X}})^{\mathrm{H}}(\mathbf{X} - \hat{\mathbf{X}})$ is calculated, where $\mathrm{rank}(\mathbf{A}) = d_1 = 2$ represents the diversity order. This can be explained by the fact that one symbol error results in two non-zero elements, which are located in different rows and columns, in $\mathbf{A}$. Hence, in $\mathbf{A}$, we can have at least 2 linearly independent rows or columns, which guarantees a diversity order of 2. We note that this is the worst case error event. If more than one symbol error occurs, a diversity order higher than 2 is always obtained.

Shifting Factor Selection: Secondly, the effect of shifting factor error on the diversity order is examined. Assume that the transmission matrix $\mathbf{X}$, with parameters $N_t = 4$, $T = 3$, $\xi = 1$, $\mathbf{t} = [1, 3, 2]^{\mathrm{T}}$, $\mathbf{a} = [2, 3, 4]^{\mathrm{T}}$, $\breve{\mathbf{s}} = [\breve{s}_1, \breve{s}_2, \breve{s}_3]^{\mathrm{T}}$, is transmitted, and $\hat{\mathbf{X}}$ is erroneously detected only with a shifting factor detection error ($\xi \rightarrow \xi_{e,}$) where $\xi_e = 2$ while data symbols, TAP, and AAP are decoded correctly. In this case, the corresponding error event can be expressed as follows:

$$\mathbf{X} \rightarrow \hat{\mathbf{X}} = \begin{bmatrix} 0 & 0 & 0 \\ \breve{s}_1^R + j\breve{s}_3^I & 0 & 0 \\ 0 & \breve{s}_3^R + j\breve{s}_2^I & 0 \\ 0 & 0 & \breve{s}_2^R + j\breve{s}_1^I \end{bmatrix} \rightarrow \begin{bmatrix} 0 & 0 & 0 \\ \breve{s}_1^R + j\breve{s}_2^I & 0 & 0 \\ 0 & \breve{s}_3^R + j\breve{s}_1^I & 0 \\ 0 & 0 & \breve{s}_2^R + j\breve{s}_3^I \end{bmatrix}. \tag{5.14}$$

For this specific error event, different from single symbol errors, three non-zero elements occur in $\mathbf{A}$ due to the erroneous shift in the imaginary parts of data symbols. Here, $\text{rank}(\mathbf{A}) = d_2 = 3$ is always obtained for this error event.

TAP Selection: The effect of TAP selection on diversity order is analyzed thirdly. Assume that the transmission matrix $\mathbf{X}$, with parameters $N_t = 4$, $T = 3$, $\xi = 1$, $\mathbf{t} = [1, 3, 2]^{\mathrm{T}}$, $\mathbf{a} = [2, 3, 4]^{\mathrm{T}}$, $\tilde{\mathbf{s}} = [\tilde{s}_1, \tilde{s}_2, \tilde{s}_3]^{\mathrm{T}}$, is transmitted, and $\hat{\mathbf{X}}$ is erroneously detected only with a TAP error ($\mathbf{t} \rightarrow \mathbf{t}_e$) where $\mathbf{t}_e = [1, 2, 3]$ is erroneously detected while the shifting factor, data symbols, and AAP are decoded correctly. In this case, the error event can be expressed as follows:

$$\mathbf{X} \rightarrow \hat{\mathbf{X}} = \begin{bmatrix} 0 & 0 & 0 \\ \tilde{s}_1 & 0 & 0 \\ 0 & \tilde{s}_3 & 0 \\ 0 & 0 & \tilde{s}_2 \end{bmatrix} \rightarrow \begin{bmatrix} 0 & 0 & 0 \\ \tilde{s}_1 & 0 & 0 \\ 0 & \tilde{s}_2 & 0 \\ 0 & 0 & \tilde{s}_3 \end{bmatrix}. \tag{5.15}$$

For this specific error event, $\text{rank}(\mathbf{A}) = d_3 = 2$ represents the diversity order. The error in TAP causes two non-zero elements, which are located in different rows and columns, in $\mathbf{A}$. Hence, A diversity order of 2 is warranted.

AAP Selection: The last step in our diversity analysis is the investigation of the effect of erroneous AAP detection on the diversity order. Assume that the transmission matrix $\mathbf{X}$, with parameters $N_t = 4$, $T = 3$, $\xi = 1$, $\mathbf{t} = [1, 3, 2]^{\mathrm{T}}$, $\mathbf{a} = [2, 3, 4]^{\mathrm{T}}$, $\tilde{\mathbf{s}} = [\tilde{s}_1, \tilde{s}_2, \tilde{s}_3]^{\mathrm{T}}$, is transmitted, and $\hat{\mathbf{X}}$ is erroneously detected only with an AAP error ($\mathbf{a} \rightarrow \mathbf{a}_e$) while shifting factor, TAP, and data symbols are decoded correctly, and $\mathbf{a}_e = [3, 4, 1]$. In this case, the error event can be expressed as follows:

$$\mathbf{X} \rightarrow \hat{\mathbf{X}} = \begin{bmatrix} 0 & 0 & 0 \\ \tilde{s}_1 & 0 & 0 \\ 0 & \tilde{s}_3 & 0 \\ 0 & 0 & \tilde{s}_2 \end{bmatrix} \rightarrow \begin{bmatrix} 0 & 0 & \tilde{s}_2 \\ 0 & 0 & 0 \\ \tilde{s}_1 & 0 & 0 \\ 0 & \tilde{s}_3 & 0 \end{bmatrix}. \tag{5.16}$$

For this specific error event, the minimum diversity order of 2 is guaranteed with $\text{rank}(\mathbf{A}) = d_4 \geq 2$.

As a result, all worst case error events are provided for different type of detection errors. Even for these worst case pairwise error events, our proposed scheme

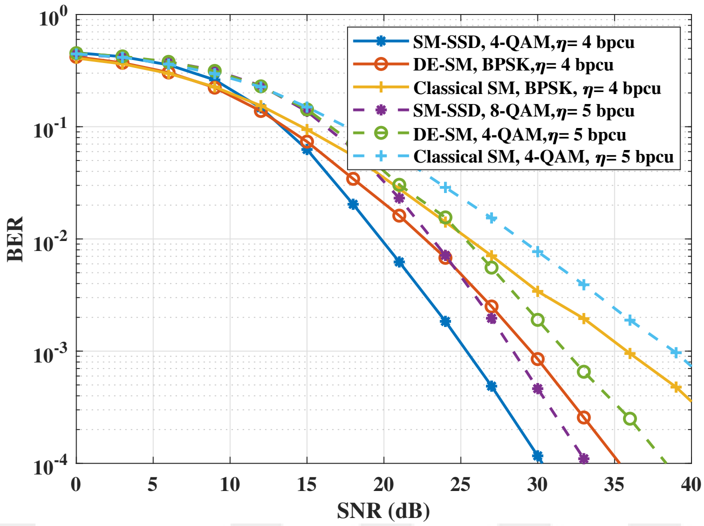

Figure 5.2: BER performance comparison of SM-SSD with benchmark schemes for a 8×1 system under 4 and 5 bpcu.

provides at least second order diversity. By induction, the other pairwise error events can be also investigated. Finally, in view of all the above, SM-SSD provides $\min_{\mathbf{X},\hat{\mathbf{X}}} \mathrm{rank}(\mathbf{A}) = 2$ which demonstrates that the diversity order of the system is 2.

5.3 Simulation Results

In this section, Monte Carlo simulations are demonstrated to compare the BER performance of SM-SSD with benchmark schemes, and the results are verified by theoretical upper bound derivations. In addition, the BER performance of SM-SSD is evaluated for the correlated and uncorrelated channels. Lastly, the variation of spectral efficiency is observed for different T and N_t values under the same modulation order.

Fig. 5.2 shows the BER performance comparison between SM-SSD for $T = 3$ and the benchmark schemes under 4 and 5 bpcu for a 8×1 system. As seen from Fig. 5.2, SM-SSD has a higher diversity order than the benchmark schemes, and having higher diversity order results in better BER performance with respect to the benchmark schemes even though SM-SSD has a higher modulation order. At the

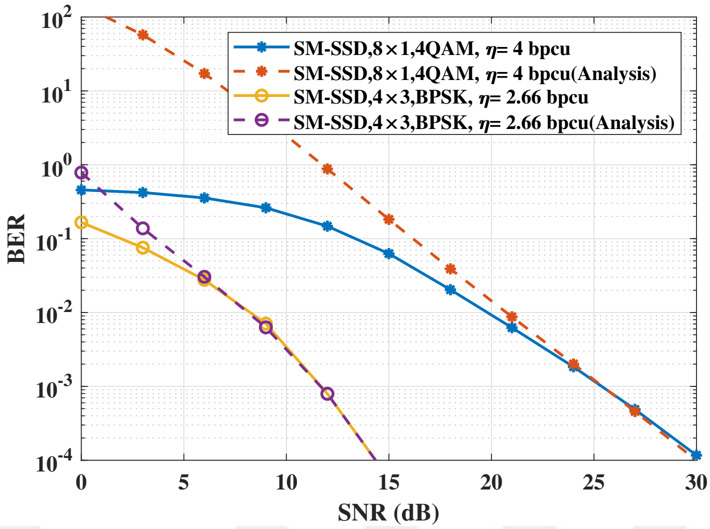

Figure 5.3: BER performance comparison of SM-SSD with theoretical results for 8×1 sytem with 4 bpcu and 4×3 system with 2.66 bpcu, respectively.

BER level of 10^{-4}, SM-SSD provides at least 5 dB SNR gain with respect to the benchmark schemes under both data rates.

Fig. 5.3 provides the BER performance comparison between the theoretical upper bound of the BER and Monte Carlo simulations for a 4×2 system with 2.66 bpcu and a 8×1 system with 4 bpcu. As seen from Fig. 5.3, the theoretical upper bound and computer simulations match at high SNR values as expected.

In Fig. 5.4, the BER performances of SM-SSD with 4-QAM and classical SM with BPSK are investigated for $\tau = 0$, 0.7, 0.9 under 4 bpcu. It is seen clearly that the increase in the channel correlation coefficient degrades the BER performances of both schemes, however, SM-SSD is stronger than classical SM against the channel correlation.

Finally, Fig. 5.5 demonstrates the variation in spectral efficiency with respect to T and N_t for $M = 4$. In Fig. 5.5(a), the spectral efficiency changes with T while $N_t = 4$ and $M = 4$. The spectral efficiency increases with T proportionally since the number of possible TAPs and ξ increases when T increases. In addition, the spectral efficiency also increases with N_t as seen in Fig. 5.5(b). However, there is a loss in spectral efficiency with respect to the benchmark schemes due to the elimination

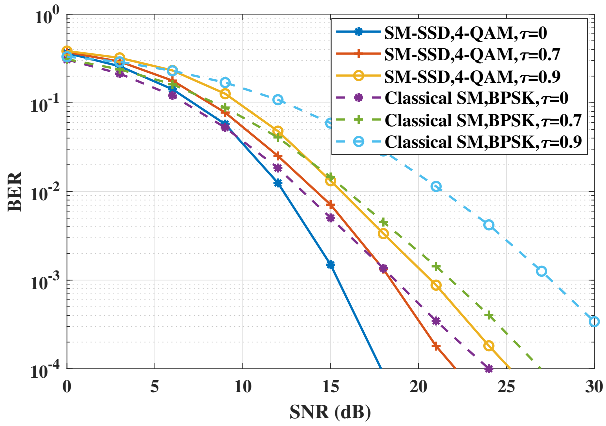

Figure 5.4: BER performance comparison of SM-SSD for a 8×2 system under 4 bpcu for different τ values.

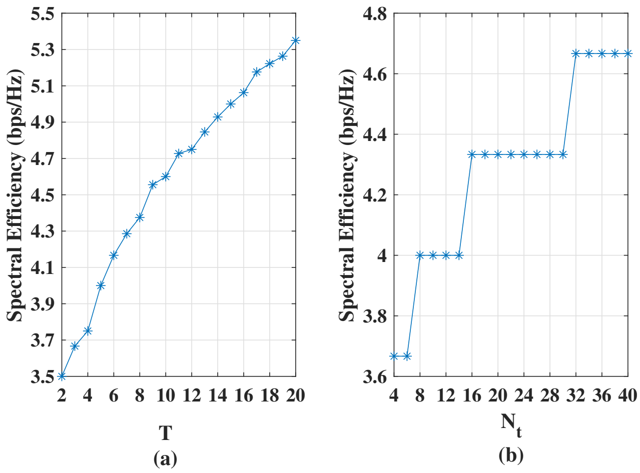

Figure 5.5: Spectral efficiency variation of SM-SSD with respect to a) T, b) N_t.

of possible AAPs to prevent transmit diversity degradation. It is transparent that there is a trade-off between the transmit diversity and the spectral efficiency.

Chapter 6

CONCLUSION

Higher spectral and energy efficiencies, low hardware and receiver complexities, and high reliable communication are the main requirements of next generation communication technologies. In this thesis, we focused on designing novel SM-based transmission schemes to meet these requirements. In this way, three novel SM-based transmission schemes are proposed for MIMO systems.

In this thesis, firstly, working principle of SM and the SM-based studies in the literature are introduced.

Secondly, TAG-QSM system model, which is designed for MIMO systems and transmits more bits with antenna indexing compared to reference system models, and enables the use of a lower modulation level with the same spectral efficiency, is introduced. The BER upper bound of the introduced scheme is expressed mathematically and compared with computer simulations. In addition, it has been shown that the TAG-QSM system model is superior to PQSM and QSM structures in terms of error performance at the same spectral efficiency.

Thirdly, a novel SM-based MIMO scheme called FSM-TAS has been introduced. The proposed scheme determines N_A by means of IM to convey additional information bits and uses transmit antennas flexibly. Transmitter and receiver complexities have been analyzed and compared with the benchmark scheme. It has been shown that a varying N_A provides lower complexity. In addition, the theoretical expression of outage probability has been derived and compared with Monte Carlo simulation for validation. The BER superiority of FSM-TAS is also shown. Finally, we conclude that FSM-TAS can be a candidate for future MIMO systems due to its improved BER performance and flexibility in the number of active antennas. The proposed idea is described for ordinary SM; however, it can also be applied for enhanced SM techniques in the future.

Lastly, a novel SM-IM-based transmission scheme called SM-SSD has been proposed for MIMO systems. SM-SSD processes multiple consecutive time slots jointly. TAP algorithm decides the placements of data symbols for the transmission. A clever shifting mechanism considering incoming bits for the imaginary parts of the rotated data symbols to apply SSD. Besides, SM-SSD generates the AAPs to enhance the transmit diversity. As a result of the transmit diversity enhancement, SM-SSD outperforms the benchmark schemes in terms of BER performance and is promising for the next generation of MIMO systems.

To conclude, the requirements of future communication systems are considered, and solutions are provided with the proposed novel schemes. These proposed schemes are promising since they provide flexibility for the use of transmit antennas, reliability and increase in data rate. In future studies, these proposed schemes would be adapted for a multiuser MIMO systems, and real-time experiments may be performed using universal software radio peripheral (USRP). In addition, low complexity detection algorithms can be designed for these proposed schemes to decrease receiver complexity.

BIBLIOGRAPHY

[Alamouti, 1998] Alamouti, S. M. (1998). A simple transmit diversity technique for wireless communications. *IEEE J. on Sel. Areas Commun.*, 16(8):1451–1458.

[Althunibat and Mesleh, 2018] Althunibat, S. and Mesleh, R. (2018). Enhancing spatial modulation system performance through signal space diversity. *IEEE Commun. Lett.*, 22(6):1136–1139.

[Basar, 2016] Basar, E. (Jul. 2016). Index modulation techniques for 5g wireless networks. *IEEE Commun. Mag.*, 54(7):168–175.

[Basar et al., 2017] Basar, E., Wen, M., Mesleh, R., Di Renzo, M., Xiao, Y., and Haas, H. (Aug.2017). Index modulation techniques for next-generation wireless networks. *IEEE Access*, 5:16693–16746.

[Boutros and Viterbo, 1998] Boutros, J. and Viterbo, E. (1998). Signal space diversity: a power-and bandwidth-efficient diversity technique for the rayleigh fading channel. *IEEE Trans. Inf. Theory*, 44(4):1453–1467.

[Datta et al., 2015] Datta, T., Eshwaraiah, H. S., and Chockalingam, A. (2015). Generalized space-and-frequency index modulation. *IEEE Transactions on Vehicular Technology*, 65(7):4911–4924.

[David and Nagaraja, 2004] David, H. A. and Nagaraja, H. N. (2004). *Order statistics*. 3rd ed. John Wiley & Sons.

[Foschini, 1996] Foschini, G. J. (1996). Layered space-time architecture for wireless communication in a fading environment when using multi-element antennas. *Bell labs technical journal*, 1(2):41–59.

[Huang et al., 2019] Huang, G., Li, C., Aïssa, S., and Xia, M. (2019). Parallel quadrature spatial modulation for massive mimo systems with ici avoidance. *IEEE Access*, 7:154750–154760.

[Jeganathan et al., 2008] Jeganathan, J., Ghrayeb, A., and Szczecinski, L. (2008). Spatial modulation: Optimal detection and performance analysis. *IEEE Communications Letters*, 12(8):545–547.

[Jeon and Lee, 2015] Jeon, C. and Lee, J. W. (2015). Multi-strata space-time coded spatial modulation. *IEEE Commun. Lett.*, 19(11):1945–1948.

[Kumbhani and Kshetrimayum, 2014] Kumbhani, B. and Kshetrimayum, R. (2014). Outage probability analysis of spatial modulation systems with antenna selection. *Electron. Lett.*, 50(2):125–126.

[Kurt and Basar, 2021] Kurt, M. A. and Basar, E. (2021). Transmit antenna grouping quadrature spatial modulation for mimo systems. In *2021 29th Signal Processing and Communications Applications Conference (SIU)*, pages 1–4.

[Kurt and Basar, 2022] Kurt, M. A. and Basar, E. (2022). Flexible spatial modulation with transmit antenna selection for mimo systems. *IEEE Systems Journal*, pages 1–4.

[Li and Wang, 2014] Li, X. and Wang, L. (2014). High rate space-time block coded spatial modulation with cyclic structure. *IEEE Commun. Lett.*, 18(4):532–535.

[Mesleh et al., 2011] Mesleh, R., Elgala, H., and Haas, H. (2011). Optical spatial modulation. *J. Opt. Commun. and Netw.*, 3(3):234–244.

[Mesleh et al., 2006] Mesleh, R., Haas, H., Ahn, C. W., and Yun, S. (2006). Spatial modulation-a new low complexity spectral efficiency enhancing technique. In *Proc. CHINACOM*, pages 1–5.

[Mesleh et al., 2014] Mesleh, R., Ikki, S. S., and Aggoune, H. M. (2014). Quadrature spatial modulation. *IEEE Trans. Veh. Technol.*, 64(6):2738–2742.

[Paulraj et al., 2003] Paulraj, A., Rohit, A. P., Nabar, R., and Gore, D. (2003). *Introduction to space-time wireless communications.* Cambridge university press.

[Pillay and Xu, 2013] Pillay, N. and Xu, H. (2013). Comments on "Antenna selection in spatial modulation systems". *IEEE Commun. Lett.*, 17(9):1681–1683.

[Popoola et al., 2013] Popoola, W. O., Poves, E., and Haas, H. (2013). Error performance of generalised space shift keying for indoor visible light communications. *IEEE Trans. on Commun.*, 61(5):1968–1976.

[Proakis, 2000] Proakis, J. G. (2000). *Digital Communications.* 4th ed. New York: McGraw-Hill.

[Qing et al., 2021] Qing, H., Yu, H., Liu, Y., and Wen, M. (2021). Enhanced spatial modulation with generalized antenna selection in MISO channels. *IET Commun.*, 15, no. 16:2046–2053.

[Rajashekar et al., 2013] Rajashekar, R., Hari, K., and Hanzo, L. (2013). Antenna selection in spatial modulation systems. *IEEE Commun. Lett.*, 17(3):521–524.

[Simon and Alouini, 2001] Simon, M. K. and Alouini, M.-S. (2001). *Digital Communication over Fading Channels.* New York: Wiley.

[Vlădeanu et al., 2012] Vlădeanu, C., Lucaciu, R., and Mihăescu, A. (2012). Optical spatial modulation for indoor wireless communications in presence of inter-symbol interference. In *2012 10th International Symposium on Electronics and Telecommunications*, pages 183–186. IEEE.

[Wang et al., 2012] Wang, J., Jia, S., and Song, J. (2012). Generalised spatial modulation system with multiple active transmit antennas and low complexity detection scheme. *IEEE Trans. Wireless Commun.*, 11(4):1605–1615.

[Yang et al., 2016] Yang, P., Xiao, Y., Guan, Y. L., Li, S., and Hanzo, L. (2016). Transmit antenna selection for multiple-input multiple-output spatial modulation systems. *IEEE Trans. Commun.*, 64(5):2035–2048.

[Yang et al., 2019] Yang, Y., Ma, P., Pang, K., Bai, Z., Han, T., and Kwak, K. (2019). Design of space signal diversity based quadrature spatial modulation. In *Proc. 19th Int. Symp. on Commun. Inf. Technol. (ISCIT)*, pages 173–177. IEEE.

[Yigit and Basar, 2016] Yigit, Z. and Basar, E. (2016). Double spatial modulation: A high-rate index modulation scheme for mimo systems. In *2016 International Symposium on Wireless Communication Systems (ISWCS)*, pages 347–351. IEEE.

[Younis et al., 2010] Younis, A., Serafimovski, N., Mesleh, R., and Haas, H. (2010). Generalised spatial modulation. In *2010 conference record of the forty fourth Asilomar conference on signals, systems and computers*, pages 1498–1502. IEEE.